materials

MDPI

Article

Si_{96}: A New Silicon Allotrope with Interesting Physical Properties

Qingyang Fan [1,*], Changchun Chai [1], Qun Wei [2], Peikun Zhou [3], Junqin Zhang [1] and Yintang Yang [1]

1 Key Laboratory of Ministry of Education for Wide Band-Gap Semiconductor Materials and Devices, School of Microelectronics, Xidian University, Xi'an 710071, China; ccchai@mail.xidian.edu.cn (C.C.); zhangjq@mail.xidian.edu.cn (J.Z.); ytyang@xidian.edu.cn (Y.Y.)

2 School of Physics and Optoelectronic Engineering, Xidian University, Xi'an 710071, China; qunwei@xidian.edu.cn

3 Faculty of Science, University of Paris-Sud, Paris 91400, France; zpkhhx@gmail.com

* Correspondence: fanqy1991@stu.xidian.edu.cn; Tel.: +86-29-8820-2507

Academic Editor: Martin O. Steinhauser

Received: 22 January 2016; Accepted: 7 April 2016; Published: 13 April 2016

Abstract: The structural mechanical properties and electronic properties of a new silicon allotrope Si_{96} are investigated at ambient pressure by using a first-principles calculation method with the ultrasoft pseudopotential scheme in the framework of generalized gradient approximation. The elastic constants and phonon calculations reveal that Si_{96} is mechanically and dynamically stable at ambient pressure. The conduction band minimum and valence band maximum of Si_{96} are at the R and G point, which indicates that Si_{96} is an indirect band gap semiconductor. The anisotropic calculations show that Si_{96} exhibits a smaller anisotropy than diamond Si in terms of Young's modulus, the percentage of elastic anisotropy for bulk modulus and shear modulus, and the universal anisotropic index A^U. Interestingly, most silicon allotropes exhibit brittle behavior, in contrast to the previously proposed ductile behavior. The void framework, low density, and nanotube structure make Si_{96} quite attractive for applications such as hydrogen storage and electronic devices that work at extreme conditions, and there are potential applications in Li-battery anode materials.

Keywords: *ab initio* calculations; structural and anisotropic properties; silicon allotropes

1. Introduction

Searching for novel silicon allotropes has been of great interest over the past several decades and has been extensively studied. In other words, it is a hot topic. Experimentally, silicon has been found to have a complicated phase diagram [1]. Many semiconductor silicon structures that have an indirect band gap have been proposed, such as the *M* phase, *Z* phase [2], *Cmmm* phase [3], body-centered-tetragonal Si [4], *M*4 phase [5], lonsdaleite phase [6], *T*12 phase [7], *ST*12 phase [8], C-centered orthorhombic phase [9], *C*2/*m*-16, *C*2/*m*-20, *Amm*2, *I*-4 [10], and $P222_1$ [11], among others. Many semiconductor silicon structures with a direct band gap have been reported, such as $P2_13$ phase [12], *oF*16-Si, *tP*16-Si, *mC*12-Si, and *tI*16-Si [13]. Silicon structures with metallic properties have also been reported, such as the *β*-Sn phase, *R*8 phase [14], and *Ibam* phase [15]. All of the previous studies have opened the possibility of a broader search for new allotropes of silicon that possibly exhibit novel properties. Karttunen *et al.* [16] have investigated the structural and electronic properties of various clathrate frameworks that are composed of the group 14 element semiconductors, including carbon, silicon, germanium, and tin. Several of the studied clathrate frameworks for silicon possess direct and wide band gaps [16]. Zwijnenburg *et al.* [17] have studied several new prospective low-energy silicon allotropes that use density functional theory, brute-force random search approaches and hypothetical 4CNs from Treacy

and co-workers. These new low-energy silicon allotropes contain 4-member rings that were previously considered to be incompatible with low-energy silicon structures, and these computational approaches that were employed to explore the energy landscape of silicon were all found to have their own optimal zone of applicability. A systematic search for silicon allotropes was performed by employing a modified *ab initio* minima hopping crystal structure prediction method by Amsler *et al.* [18]. They found silicon clathrates that had low density and a stronger overlap of the absorption spectra with the solar spectrum compared to conventional diamond silicon, which are thus promising candidates for use in thin-film photovoltaic applications. Recently, Li *et al.* [19] found a novel cubic allotrope of carbon, C_{96}-carbon, that has intriguing physical properties. We proposed Si_{96} (space group: *Pm*-3*m*), whose structure is based on C_{96}-carbon [19], with silicon atoms substituting carbon atoms. The physical properties of this new cubic Si allotrope are reported in this paper. The Si_{96} is composed of six-membered silicon rings that are very similar to graphite-like six-membered carbon rings. Furthermore, the structure of the cubic Si_{96} phase is porous and has a lower density. Due to its structural porous feature and lower density, Si_{96} can also be expected to be good hydrogen storage material. The calculation of the Mulliken overlap population ensures the existence of strong covalent bonds in six-membered silicon rings, and thus, the hardness of Si_{96} is close to diamond Si. Six-membered silicon rings and zigzag six-membered silicon rings cause Si_{96} to have a lower density among the silicon allotrope materials.

2. Materials and Methods

All of the calculations are performed by utilizing the generalized gradient approximation (GGA) functional in the Perdew, Burke and Ernzerrof (PBE) [20] functional form in Cambridge sequential total energy package (CASTEP) [21]. The core-valence interactions were described as Ultra-soft pseudopotentials [22]. The Broyden–Fletcher–Goldfarb–Shanno (BFGS) [23] minimization scheme was used in geometric optimization. The valence electron configurations of Si $3s^2 3p^2$ are considered. A tested mesh of $4 \times 4 \times 4$ *k*-point sampling was used for the calculations. For the new Si phase, the ultrasoft pseudopotential was used with the cutoff energy of 300 eV. The self-consistent convergence of the total energy is 5×10^{-6} eV/atom; the maximum force on the atom is 0.01 eV/Å, the maximum ionic displacement is within 5×10^{-4} Å, and the maximum stress is within 0.02 GPa. Both the HSE06 hybrid functional [24] and GGA-PBE methods were used for the calculations of electronic structures. The phonon spectra of Si_{96} used the linear response approach, also called density functional perturbation theory (DFPT), which is one of the most popular methods of an *ab initio* calculation of lattice dynamics [25].

3. Results and Discussion

The crystal structure of Si_{96} is shown in Figure 1; it belongs to the *Pm*-3*m* space group of cubic symmetry. The basic building blocks of Si_{96} are six-membered graphite-like carbon rings, which can be clearly observed in Figure 1a. The six-membered rings are normal to the [111] direction in the structure of Si_{96} (Figure 1b). The optimized equilibrium lattice parameter is a = 13.710 Å at ambient pressure, and there are 96 silicon atoms in a conventional cell. The three color spheres represent three non-equivalent atoms. The blue atoms occupy the crystallographic 48*n* sites in a conventional cell, which is (0.6605, 0.7863, 0.0870). The red atoms occupy the crystallographic $24l_1$ sites in a conventional cell, which is (0.3792, 0.5, 0.2580). The cyan atoms also occupy the crystallographic $24l_2$ sites, which have the (0.5, 0.7143, 0.1373) position in a conventional cell, respectively. Furthermore, Si_{96} has nanotube-like cavities along the crystallographic main axis and the [111] direction, as shown in Figure 1a,b. It is well known that the regular arrangement of nanotubes can enhance the efficiency of the hydrogen storage of nanotubes [19]. Thus, the Si_{96} can be expected to have a good ability for hydrogen storage. Generally, the densities of the materials are closely related to the hydrogen storage ability of materials. The density (1.737 g/cm^3) of Si_{96} is smaller than that of diamond Si (calculated value: 2.322 g/cm^3, experimental value: 2.329 g/cm^3). In addition, the densities of *I*-4 (2.1511 g/cm^3), *Amm*2 (2.1809 g/cm^3), *C*2/*m*-16 (2.2172 g/cm^3), *C*2/*m*-20 (2.2251 g/cm^3) [10] and $P222_1$ (2.227 g/cm^3) [11] are slightly larger than that

of Si_{96}. Thus, Si_{96} can be expected to have a good hydrogen storage ability among the low density materials or potential applications to Li-battery anode materials.

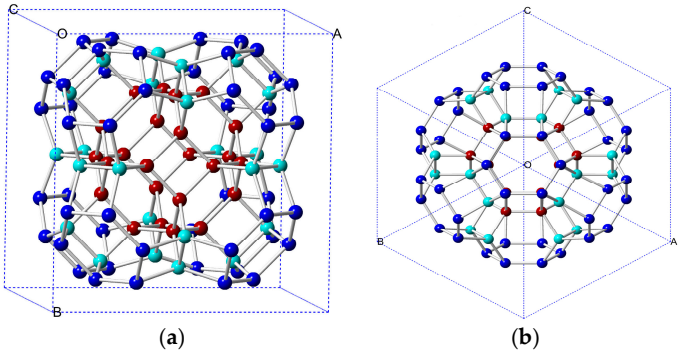

(**a**) (**b**)

Figure 1. Unit cell crystal structures of Si_{96} (**a**) and along the [111] direction (**b**).

There are eight bond lengths in Si_{96}, namely, 2.3397, 2.3398, 2.3514, 2.3557, 2.3858, 2.3873, 2.4419 and 2.4540 Å, and each bond length has a difference number; the average bond length is 2.3862 Å, which is slightly larger than that of diamond Si (2.3729 Å). The atoms occupy the crystallographic $24l_1$ sites, which consist of a four-membered ring. The four bond lengths are all 2.3398 Å. The other atoms occupy the crystallographic $24l_1$ sites, which consist of a six-membered silicon ring. The six-membered ring includes two bond lengths, 2.3514 and 2.3398 Å. Some of the atoms that occupy the crystallographic $24l_2$ sites are connected to occupy the crystallographic $24l_1$ sites and $48n$ sites, and the bond lengths are 2.3397 and 2.3873 Å, respectively. Some of the atoms that occupy the crystallographic $24l_2$ sites connect to themselves, and the bond length is 2.3557 Å. The other six-membered silicon ring consists of the atoms that occupy the crystallographic $48n$ sites, and it includes two bond lengths, 2.4419 and 2.4540 Å. Moreover, there is a zigzag six-membered silicon ring that consists of the three non-equivalent atoms, which includes three bond lengths, 2.3397, 2.3873 and 2.4419 Å.

To understand the thermodynamic stability, the enthalpies of the proposed structures were compared with the experimentally known diamond Si and β-Sn phase Si and the theoretically proposed M phase, Z phase, lonsdaleite phase, $P4_2/ncm$ phase, C-centered orthorhombic (Cco) phase, $P4_2/mnm$ phase, and $P4_2/mmc$ phase ($tP16$-Si), as depicted in Figure 2. It is obvious that diamond Si remains the most stable phase at ambient pressure. The most unfavorable Si_{96} is higher in energy than diamond Si by 0.307 eV/atom at ambient pressure, while the metastable lonsdaleite phase is 0.017 eV/atom higher than diamond Si. In Ref. [13], the most unfavorable $tP16$-Si is higher in energy than diamond Si by 0.269 eV/atom (this work: 0.277 eV/atom) at ambient pressure. In Ref. [12], the new Si_{20} structure (space group: $P2_13$) is less stable than Fd-$3m$ Si by approximately 0.3 eV/Si due to the distortion of the Si tetrahedrons. Generally, the distortion of the tetrahedron in these metastable structures leads to their higher energy. The planar four-membered silicon rings will result in a more severe distortion than five-membered silicon rings. The dynamical stability of the structure of Si_{96} was checked in this paper. The phonon dispersion for Si_{96} at ambient pressure was calculated. No imaginary frequencies are observed throughout the whole Brillouin zone, which signals dynamically the structural stability of Si_{96}, as shown in Figure 3.

In addition, we calculated the hardness of Si_{96} and diamond Si using the model of Lyakhov and Oganov [26]. The hardness of Si_{96} is 9.6 GPa, which is slightly smaller than that of diamond Si (13.3 GPa). The other results of hardness for diamond Si are 8 GPa [27], 9 GPa [28], 12.4 GPa [29], and 2–16 GPa [30]. To understand the origin of the hardness, it is necessary to understand the Mulliken overlap population and bond length. The average bond length of Si_{96} is 2.3862 Å, a value that is very close to that of diamond Si, which indicates that the bonds of Si_{96} should have as high a bond strength as that of diamond. The average Mulliken overlap population of Si_{96} (0.66) is very close to that of diamond Si (0.73), which also confirms that the bond strength of Si_{96} is very strong.

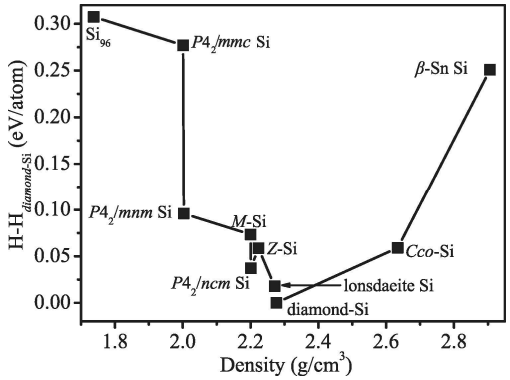

Figure 2. Calculated enthalpies of different silicon structures relative to the diamond Si at ambient pressure.

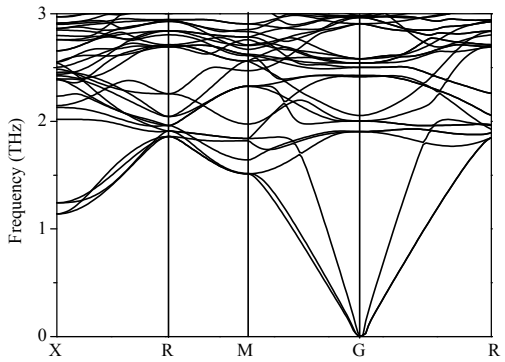

Figure 3. Phonon spectrum for Si_{96}.

We next investigate the mechanical properties of Si_{96} and diamond Si for reference. The calculated results of Si_{96} and diamond Si are listed in Table 1. The three independent elastic constants C_{ij} of the cubic symmetry, namely C_{11}, C_{12}, and C_{44}, obey the following generalized Born's mechanical stability criteria: $C_{11} > 0$, $C_{44} > 0$, C_{11}-$C_{12} > 0$, and $C_{11} + 2C_{12} > 0$ [31,32]. The elastic modulus is also calculated. Young's modulus E and Poisson's ratio v are taken as follows: $E = 9BG/(3B + G)$, $v = (3B - 2G)/[2(3B + G)]$. The bulk modulus and shear modulus are smaller than that of diamond Si. The shear modulus and Young's modulus of Si_{96} is only approximately one third that of diamond Si. In addition, the value of Poisson's ratio is larger than that of diamond Si. Pugh [33] proposed the ratio of bulk to shear modulus (B/G) as an indication of ductile *versus* brittle characters. If $B/G > 1.75$, then the material behaves in a ductile way. Otherwise, the material behaves in a brittle way. The B/G of Si_{96} is larger than 1.75, which suggests that the Si_{96} allotrope is prone to ductile behavior. Interestingly, most of the silicon allotropes exhibit brittle behavior (M-Si: 1.22; Z-Si: 1.35; T_{12}-Si: 1.56; I-4: 1.68; $Amm2$: 1.54, $C2/m$-16 Si: 1.60; $C2/m$-20 Si: 1.50; $P222_1$ Si: 1.54 and diamond Si: 1.40), which contrasts with the previously proposed ductile behavior.

Table 1. The lattice parameters (Å), density (ρ: g/cm^3), elastic constants (GPa) and elastic modulus (GPa) of Si_{96} and diamond Si.

Materials	Work	*a*	ρ	C_{11}	C_{12}	C_{44}	*B*	*G*	*B*/*G*	*E*	*v*
Si_{96}	This work	13.710	1.737	89	33	26	52	27	1.93	69	0.28
Diamond Si	This work	5.436	2.322	165	65	87	98	70	1.40	170	0.21
Diamond Si	Experimental	5.431 [1]	2.329 [2]	166 [3]	64	80	102	-	-	-	-

[1] Ref. [34] at 300 K; [2] Ref. [35] at 300 K; [3] Ref. [36].

It is well known that the electronic structure determines the fundamental physical and chemical properties of materials. The calculated electronic band structures for Si_{96} utilizing GGA-PBE and HSE06 are presented in Figure 4. The electronic band structure calculation shows that the new silicon allotrope Si_{96} is metallic because the conduction band minimum and valence band maximum both overlap the Fermi level. It is known that the calculated band gap with DFT is usually underestimated by 30%–50%, and the true band gap must be larger than the calculated results. In consideration of this problem, Heyd *et al.* proposed a more tractable hybrid functional method, which gave rise to the Heyd–Scuseria–Ernzerhof (HSE06) functional. The hybrid functional HSE06 is used in the following form [37,38]:

$$E_{xc}^{HSE} = \mu E_x^{HF,SR}(\omega) + (1-\mu)E_x^{PW91,SR}(\omega) + E_x^{PW91,LR}(\omega) + E_c^{PW91} \quad (1)$$

where the HF mixing parameter μ is 0.25, and the screening parameter that provides good accuracy for the band gaps is $\omega = 0.207$ Å^{-1} [24,38]. The electronic band structure calculation shows that Si_{96} is an indirect band gap semiconductor with a band gap of 0.474 eV for the HSE06 hybrid functional. Thus, the band structure calculations show that the new Si_{96} is a narrow band gap semiconductor material.

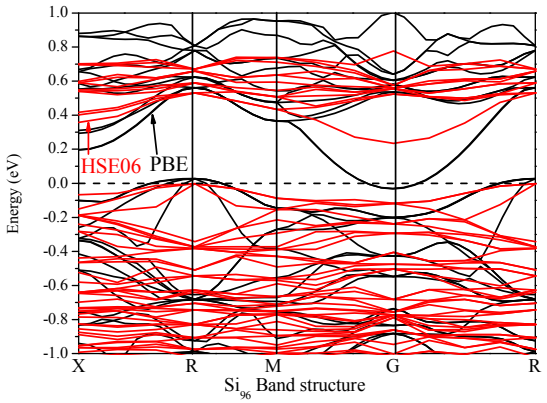

Figure 4. Electronic band structure using Perdew, Burke and Ernzerrof (PBE) and Heyd–Scuseria–Ernzerhof (HSE06) of Si_{96}.

The 3D figures of the directional dependences of the reciprocals of Young's modulus and the projections of Young's modulus at different crystal planes for the new silicon allotrope Si_{96} and diamond Si are demonstrated in Figures 5a,c and 5b,d. The three-dimensional (3D) surface construction is a valid method for describing the elastic anisotropic behavior of a solid perfectly. Usually, the anisotropic properties of materials are different due to their various crystal structures [39]. The 3D figure appears to be a spherical shape for an isotropic material, while the deviation from the spherical shape exhibits the content of anisotropy [40]. It is clear that the diamond Si exhibits greater anisotropy than that of Si_{96}. The maximal and minimal value of diamond Si are 183 and 124 GPa. The maximal and minimal value of Si_{96} are 70 and 67 GPa, respectively. $E_{max}/E_{min(diamond\ Si)}$ is equal to 1.476 and $E_{max}/E_{min(Si96)}$ is equal to 1.048, and thus, the diamond Si exhibits greater anisotropy in Young's modulus than that of Si_{96}. In addition, the elastic anisotropy of a crystal can be depicted in many different ways. In this work, several anisotropic indices are also calculated, such as the percentage of anisotropy (A_B and A_G) and the universal anisotropic index (A^U). In cubic symmetry, $B_V = B_R = (C_{11} + 2C_{12})/3$, $G_V = (C_{11} - C_{12} + 3C_{44})/5$, and $G_R = [5(C_{11} - C_{12})C_{44}]/(4C_{44} + 3C_{11} - 3C_{12})$. The equations used can be expressed as follows: $A_B = [(B_V - B_R)/(B_V + B_R)] \times 100\%$, $A_G = [(G_V - G_R)/(G_V + G_R)] \times 100\%$ and $A^U = 5G_V/G_R + B_V/B_R - 6$, and there, A^U must be greater than or equal to zero. An A^U fluctuation away from zero indicates high anisotropic elastic properties. $A_B = 0$, $A_G = 3.58\%$, and $A^U = 0.336$ for diamond Si, and $A_B = 0$, $A_G = 0.036\%$, and $A^U = 0.004$ for Si_{96}. In other words, diamond Si exhibits greater anisotropy in Young's modulus, A_B, A_G and A^U than Si_{96}.

To understand the possibility of using Si_{96} for hydrogen storage and lithium-battery anode material, we inset one and two hydrogen or lithium atoms into diamond Si (8 silicon atoms per conventional cell) and Si_{96} (96 silicon atoms per conventional cell). This method is consistent with references [5,41] to verify whether M4 silicon, diamond Si and other amorphous silicon can be used as lithium battery electrode materials. For one hydrogen (lithium) atom insertion, the volume expansion of the Si_{96} is −0.52% (−0.25%), which is much smaller than that of diamond Si (hydrogen 1.95%; lithium 2.91%, 2.94% [5]), Bct-Si (lithium 1.41% [5]) and M4-Si (lithium 1.65% [5]). For two hydrogen (lithium) atom insertions, the volume expansion of the Si_{96} is −1.18% (−0.83%), which is much smaller than that of diamond-Si (hydrogen 4.81%; lithium 7.49%, 7.53% [5]). These results show that Si_{96} has a higher capacity as a hydrogen storage and lithium-battery anode material.

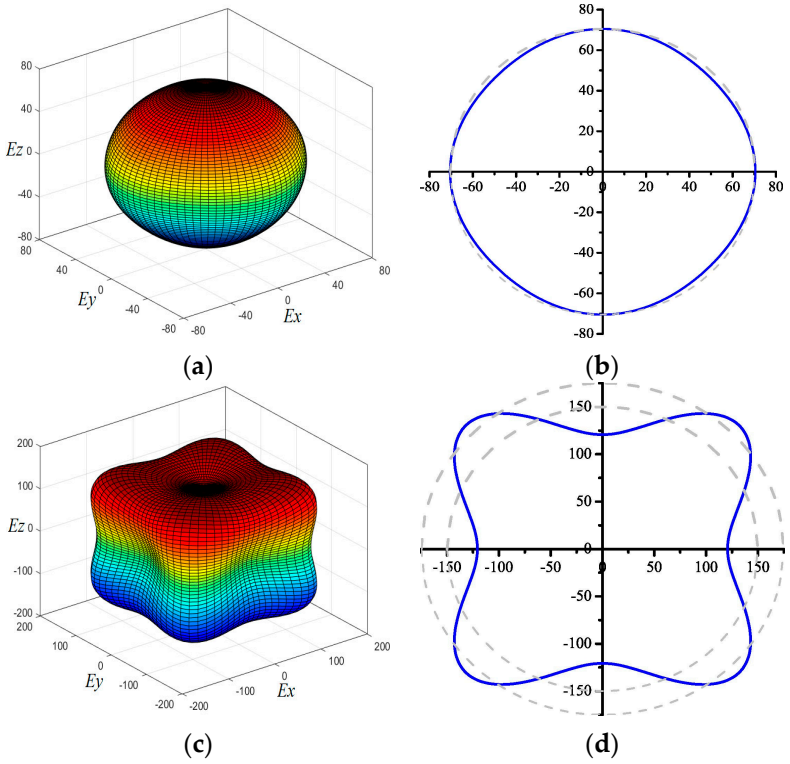

Figure 5. The directional dependence of Young's modulus for Si_{96} (**a**) and diamond Si (**c**); and a 2D representation of Young's modulus in the *xy* plane for Si_{96} (**b**) and diamond Si (**d**).

4. Conclusions

In summary, a new silicon allotrope with space group *Pm*-3*m* is predicted, which is mechanically and dynamically stable at ambient pressure. The Si_{96} is an indirect-gap semiconductor with a band gap of 0.474 eV. The 3D surface contour of Young's modulus is plotted to verify the elastic anisotropy of Si_{96} and diamond Si. At the same time, diamond Si exhibits greater anisotropy than Si_{96} in Young's modulus and a slice of anisotropic indices. The void framework, low density and nanotube structures make Si_{96} quite attractive for particular applications, such as hydrogen storage and electronic devices that work at extreme conditions, and for potential applications to Li-battery anode materials.

Acknowledgments: This work was supported by the Natural Science Foundation of China (No. 61474089), Open Fund of Key Laboratory of Complex Electromagnetic Environment Science and Technology, China Academy of Engineering Physics (No. 2015-0214. XY.K).

Author Contributions: Qingyang Fan designed the project; Qingyang Fan, Changchun Chai and Qun Wei performed the calculations; Qingyang Fan, Qun Wei, Junqin Zhang, Yintang Yang and Peikun Zhou analyzed the results; and Qingyang Fan and Changchun Chai wrote the manuscript.

Conflicts of Interest: The authors declare no conflict of interest.

References

1. Mujica, A.; Rubio, A.; Munoz, A.; Needs, R.J. High-pressure phases of group-IV, III-V, and II-VI compounds. *Rev. Mod. Phys.* **2003**, *75*, 863–912. [CrossRef]
2. Bautista-Hernandez, A.; Rangel, T.; Romero, A.H.; Rignanese, G.M.; Salazar-Villanueva, M.; Chigo-Anota, E. Structural and vibrational stability of *M* and *Z* phases of silicon and germanium from first principles. *J. Appl. Phys.* **2013**, *113*, 193504. [CrossRef]
3. Amsler, M.; Flores-Livas, J.A.; Lehtovaara, L.; Balima, F.; Ghasemi, S.A.; Machon, D.; Pailhes, S.; Willand, A.; Caliste, D.; Botti, S.; *et al.* Crystal Structure of Cold Compressed Graphite. *Phys. Rev. Lett.* **2012**, *108*, 065501. [CrossRef] [PubMed]
4. Fujimoto, Y.; Koretsune, T.; Saito, S.; Miyake, T.; Oshiyama, A. A new crystalline phase of four-fold coordinated silicon and germanium. *New J. Phys.* **2008**, *10*, 083001. [CrossRef]
5. Wu, F.; Jun, D.; Kan, E.J.; Li, Z.Y. Density functional predictions of new silicon allotropes: Electronic properties and potential applications to Li-battery anode materials. *Solid State Commun.* **2011**, *151*, 1228–1230. [CrossRef]
6. De Amrit Pryor, C.E. Electronic structure and optical properties of Si, Ge and diamond in the lonsdaleite phase. *J. Phys. Condens. Matter* **2014**, *26*, 045801. [CrossRef]
7. Zhao, Z.S.; Tian, F.; Dong, X.; Li, Q.; Wang, Q.Q.; Wang, H.; Zhong, X.; Xu, B.; Yu, D.; He, J.L.; *et al.* Tetragonal allotrope of group 14 Elements. *J. Am. Chem. Soc.* **2012**, *134*, 12362–12365. [CrossRef] [PubMed]
8. Malone, B.D.; Sau, J.D.; Cohen, M.L. *Ab initio* survey of the electronic structure of tetrahedrally bonded phases of silicon. *Phys. Rev. B* **2008**, *78*, 035210. [CrossRef]
9. Zhao, Z.S.; Xu, B.; Zhou, X.F.; Wang, L.M.; Wen, B.; He, J.L.; Liu, Z.Y.; Wang, H.T.; Tian, Y.J. Novel Superhard Carbon: C-Centered Orthorhombic C_8. *Phys. Rev. Lett.* **2011**, *107*, 215502. [CrossRef] [PubMed]
10. Fan, Q.Y.; Chai, C.C.; Wei, Q.; Yan, H.Y.; Zhao, Y.B.; Yang, Y.T.; Yu, X.H.; Liu, Y.; Xing, M.J.; Zhang, J.Q.; *et al.* Novel silicon allotropes: Stability, mechanical, and electronic properties. *J. Appl. Phys.* **2015**, *118*, 185704. [CrossRef]
11. Fan, Q.Y.; Chai, C.C.; Wei, Q.; Yang, Y.T.; Yang, Q.; Chen, P.Y.; Xing, M.J.; Zhang, J.Q.; Yao, R.H. Prediction of novel phase of silicon and Si–Ge alloys. *J. Solid State Chem.* **2016**, *233*, 471–483. [CrossRef]
12. Xiang, H.J.; Huang, B.; Kan, E.J.; Wei, S.H.; Gong, X.G. Towards direct-gap silicon phases by the inverse band structure design approach. *Phys. Rev. Lett.* **2013**, *110*, 118702. [CrossRef] [PubMed]
13. Wang, Q.Q.; Xu, B.; Sun, J.; Liu, H.Y.; Zhao, Z.S.; Yu, D.L.; Fan, C.Z.; He, J.L. Direct band gap silicon allotropes. *J. Am. Chem. Soc.* **2014**, *136*, 9826–9829. [CrossRef] [PubMed]
14. Pfrommer, B.G.; Cote, M.; Louie, S.G.; Cohen, M.L. *Ab initio* study of silicon in the R8 phase. *Phys. Rev. B* **1997**, *56*, 6662. [CrossRef]
15. Malone, B.D.; Cohen, M.L. Prediction of a metastable phase of silicon in the Ibam structure. *Phys. Rev. B* **2012**, *85*, 024116. [CrossRef]
16. Karttunen, A.J.; Fassler, T.F.; Linnolahti, M.; Pakkanen, T.A. Structural principles of semiconducting group 14 clathrate frameworks. *Inorg. Chem.* **2011**, *50*, 1733–1742. [CrossRef] [PubMed]
17. Zwijnenburg, M.A.; Jelfsab, K.E.; Bromley, S.T. An extensive theoretical survey of low-density allotropy in silicon. *Phys. Chem. Chem. Phys.* **2010**, *12*, 8505–8512. [CrossRef] [PubMed]
18. Amsler, M.; Botti, S.; Marques, M.A.L.; Lenosky, T.J.; Goedecker, S. Low-density silicon allotropes for photovoltaic applications. *Phys. Rev. B* **2015**, *92*, 014101. [CrossRef]
19. Li, D.; Tian, F.B.; Chu, B.H.; Duan, D.F.; Wei, S.L.; Lv, Y.Z.; Zhang, H.D.; Wang, L.; Lu, N.; Liu, B.B.; *et al.* Cubic C_{96}: A novel carbon allotrope with a porous nanocube network. *J. Mater. Chem. A* **2015**, *3*, 10448–10452. [CrossRef]
20. Perdew, J.P.; Burke, K.; Ernzerhof, M. Generalized gradient approximation made simple. *Phys. Rev. Lett.* **1996**, *77*, 3865–3868. [CrossRef] [PubMed]
21. Clark, S.J.; Segall, M.D.; Pickard, C.J.; Hasnip, P.J.; Probert, M.I.J.; Refson, K.; Payne, M.C. First principles methods using CASTEP. *Z. Kristallogr.* **2005**, *220*, 567–570. [CrossRef]
22. Vanderbilt, D. Soft self-consistent pseudopotentials in a generalized eigenvalue formalism. *Phys. Rev. B* **1990**, *41*, 7892–7895. [CrossRef]

23. Pfrommer, B.G.; Côté, M.; Louie, S.G.; Cohen, M.L. Relaxation of crystals with the quasi-Newton method. *J. Comput. Phys.* **1997**, *131*, 233–240. [CrossRef]
24. Krukau, A.V.; Vydrov, O.A.; Izmaylov, A.F.; Scuseria, G.E. Influence of the exchange screening parameter on the performance of screened hybrid functionals. *J. Chem. Phys.* **2006**, *125*, 224106. [CrossRef] [PubMed]
25. Baroni, S.; Gironcoli, S.; de Corso, A.; dal Giannozzi, P. Phonons and related crystal properties from density-functional perturbation theory. *Rev. Mod. Phys.* **2001**, *73*, 515–564. [CrossRef]
26. Lyakhov, A.O.; Oganov, A.R. Evolutionary search for superhard materials: Methodology and applications to forms of carbon and TiO_2. *Phys. Rev. B* **2011**, *84*, 092103. [CrossRef]
27. Gilman, J.J. Flow of covalent solids at low temperatures. *J. Appl. Phys.* **1975**, *46*, 5110–5113. [CrossRef]
28. Lawn, B.R.; Evans, A.G.; Marshall, D.B. Elastic/Plastic Indentation Damage in Ceramics: The Median/Radial Crack System. *J. Am. Ceram. Soc.* **1980**, *63*, 574–581. [CrossRef]
29. Danyluk, S.; Lim, D.S.; Kalejs, J. Microhardness of carbon-doped (111) p-type Czochralski silicon. *J. Mater. Sci. Lett.* **1985**, *4*, 1135–1137. [CrossRef]
30. Feltham, P.; Banerjee, R. Theory and application of microindentation in studies of glide and cracking in single crystals of elemental and compound semiconductors. *J. Mater. Sci.* **1992**, *27*, 1626–1632. [CrossRef]
31. Wu, Z.J.; Zhao, E.J.; Xiang, H.P.; Hao, X.F.; Liu, X.J.; Meng, J. Crystal structures and elastic properties of superhard IrN_2 and IrN_3 from first principles. *Phys. Rev. B* **2007**, *76*, 054115. [CrossRef]
32. Fan, Q.Y.; Wei, Q.; Yan, H.Y.; Zhang, M.G.; Zhang, D.Y.; Zhang, J.Q. A New Potential Superhard Phase of OsN_2. *Acta Phys. Pol. A* **2014**, *126*, 740–746. [CrossRef]
33. Pugh, S.F. XCII. Relations between the elastic moduli and the plastic properties of polycrystalline pure metals. *Lond. Edinb. Dublin Philosop. Mag. J. Sci. Ser.* **1954**, *45*, 823–843. [CrossRef]
34. Basile, G.; Bergamin, A.; Cavagenro, G.; Mana, G.; Vittone, E.; Zosi, G. Measurement of the silicon (220) lattice spacing. *Phys. Rev. Lett.* **1994**, *72*, 3133–3136. [CrossRef] [PubMed]
35. Adachi, S. Group-IV semiconductors. In *Handbook on Physical Properties of Semiconductors*; Kluwer Academic Publishers: Boston, MA, USA, 2004; Volume 2, p. 46.
36. Gomez-Abal, R.; Li, X.; Scheffler, M.; Ambrosch-Draxl, C. Influence of the core-valence interaction and of the pseudopotential approximation on the electron self-energy in semiconductors. *Phys. Rev. Lett.* **2008**, *101*, 106404. [CrossRef] [PubMed]
37. Heyd, J.; Scuseria, G.E.; Ernzerhof, M. Hybrid functionals based on a screened Coulomb potential. *J. Chem. Phys.* **2003**, *118*, 8207–8215. [CrossRef]
38. Heyd, J.; Scuseria, G.E.; Ernzerhof, M. Erratum: "Hybrid functionals based on a screened Coulomb potential" [J. Chem. Phys. 118, 8207 (2003)]. *J. Chem. Phys.* **2006**, *124*, 219906. [CrossRef]
39. Duan, Y.H.; Sun, Y.; Peng, M.J.; Zhou, S.G. Anisotropic elastic properties of the Ca–Pb compounds. *J. Alloys Compd.* **2014**, *595*, 14–21. [CrossRef]
40. Hu, W.C.; Liu, Y.; Li, D.J.; Zeng, X.Q.; Xu, C.S. First-principles study of structural and electronic properties of *C*14-type Laves phase Al_2Zr and Al_2Hf. *Comput. Mater. Sci.* **2014**, *83*, 27–34. [CrossRef]
41. Jung, S.C.; Han, Y.K. *Ab initio* molecular dynamics simulation of lithiation-induced phase-transition of crystalline silicon. *Electrochim. Acta* **2012**, *62*, 73–76. [CrossRef]